Abundant nitrogenous secondary organic aerosol formation accelerated by cloud processing

Z. Liu, B. Zhu, C. Zhu, T. Ruan, J. Li, H. Chen, Q. Li, X. Wang, L. Wang, Y. Mu, et al.

iScience

CellPress
OPEN ACCESS

Article

Abundant nitrogenous secondary organic aerosol formation accelerated by cloud processing

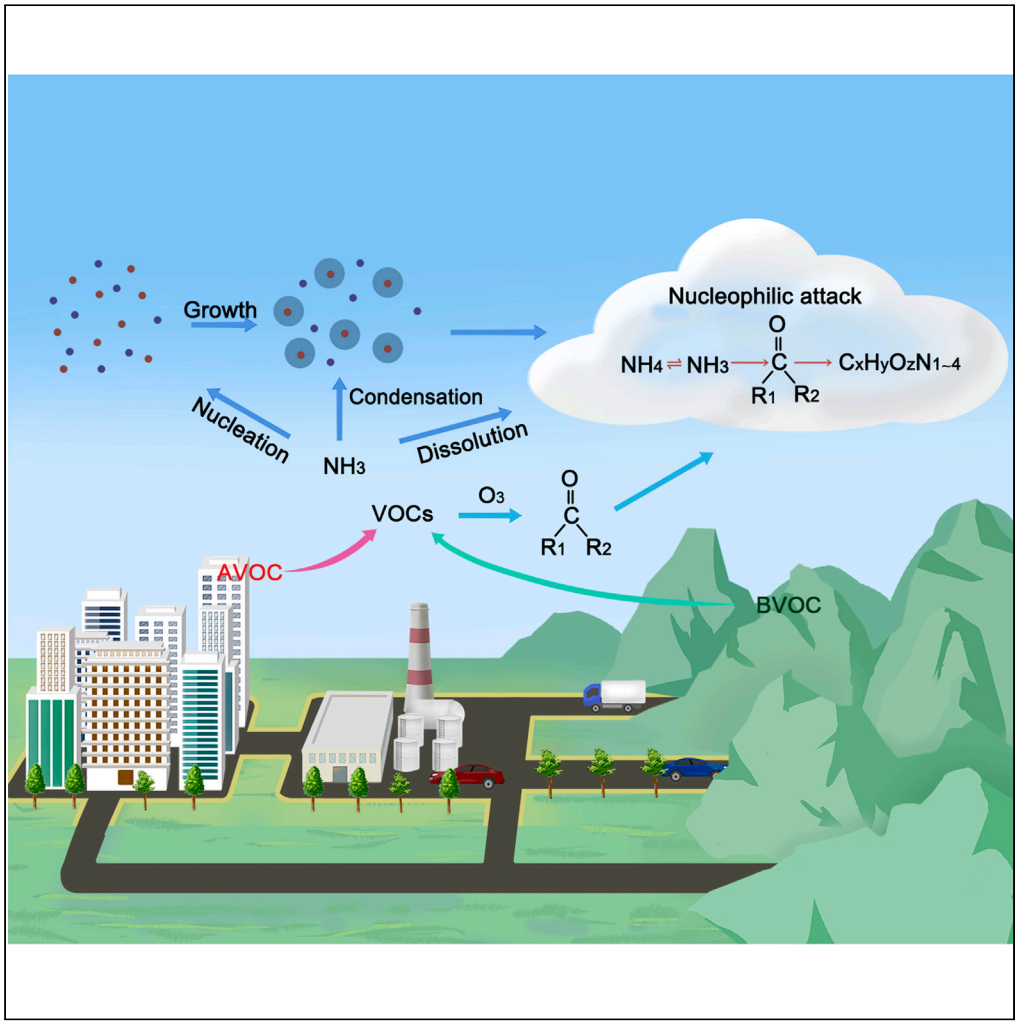

Zhe Liu, Bao Zhu, Chao Zhu, ..., Abdewahid Mellouki, Jianmin Chen, Guibin Jiang

tingruan@rcees.ac.cn (T.R.)
jmchen@fudan.edu.cn (J.C.)

Highlights

CHON transformation during CPs have been explored

CPs enhance the variety of CHONs in cloud water

CHONs formed during CPs can be represented using $C_nH_{(2n-16)-(2n)}O_{1-10}N_{1-4}$

Reaction between NH_3 and carbonyls as a possible way for the formation of CHONs

Liu et al., iScience *26*, 108317
November 17, 2023
https://doi.org/10.1016/j.isci.2023.108317

iScience

CellPress
OPEN ACCESS

Article

Abundant nitrogenous secondary organic aerosol formation accelerated by cloud processing

Zhe Liu,[1,9] Bao Zhu,[2,9] Chao Zhu,[1,9] Ting Ruan,[2,*] Jiarong Li,[1] Hui Chen,[1] Qing Li,[1] Xiaofei Wang,[1] Lin Wang,[1] Yujing Mu,[2] Jeffrey Collett, Jr.,[3] Christian George,[1,4] Yan Wang,[5] Xinfeng Wang,[5] Jixin Su,[5] Shaocai Yu,[6] Abdewahid Mellouki,[7] Jianmin Chen,[1,8,10,*] and Guibin Jiang[2]

SUMMARY

Nitrogenous organic (CHON), crucial for secondary organic aerosol (SOA), forms through poorly studied mechanisms in clouds. Our study explores CHON transformation during cloud processes (CPs). These processes play a vital role in enhancing the variety of CHONs, leading to the formation of CHONs with oxygen atom counts ranging from 1 to 10 and double bond equivalent (DBE) values spanning from 2 to 10. We proposed that the CHONs formed during CPs are formed through aqueous phase reactions with CHO compound precursors via nucleophilic attacks by NH_3. This scheme can be account for roughly three-quarters of the CHONs by number in cloud water, and near two-thirds of all CHONs are formed through reactions between NH_3 and carbonyl-containing biogenic volatile organic compound (BVOC) ozonolysis intermediates. This study provides the first insights into the evolution of CHONs during CPs and reveals the significant roles of CPs in the formation of CHONs.

INTRODUCTION

Cloud droplets contain a blend of organic and inorganic compounds formed through the scavenging of hygroscopic particles and the condensation of vapor species.[1] Clouds can significantly affect the Earth's climate by scattering solar radiation. They provide important aqueous environments in which aqueous secondary organic aerosols can form through radical reactions, inorganic–organic reactions, photochemistry, hydrolysis, and oligomerization.[2] Due to differences in the pH value, water content, and microphysics, different chemical processes may dominate in cloud water vs. aerosols, producing different organic compound compositions between these two environments.[2,3] In addition, during the evaporation of cloud droplets, increased concentration and acidity may promote reactions such as acid-catalyzed processes and condensation.[4] For example, chemical reactions between carbonyl species and ammonia have been shown to occur in evaporating droplets, an important illustration of inorganic–organic reactions in the liquid phase.[5]

Nitrogenous organics (CHONs) generally contribute up to 10–40% of the organic content of ambient aerosol particles and influence cloud condensation nuclei formation, submicron particle growth, radiative forcing, and air quality.[6–8] The formation of CHONs is perceived to be a synergistic effect of the interactions between anthropogenic/natural organic compounds and reactive nitrogen precursor emissions. These atmospheric processes involving complex atmospheric multiphase chemistry, heterogeneous reactions, and photochemical conjugations with oxidative species such as O_3, H_2O_2, OH, and NO_3.[9,10] The formation and variations of CHONs and their precursors have been widely investigated in simulation chambers and campaigns using state-of-the-art instrumental methods.[11,12] Clouds are known to be active processors of atmospheric organic matter.[13] Recent research has provided preliminary insights into molecular-level processes about CHONs in cloud water via high-resolution mass spectrometry techniques and has revealed the diversity of the compositions of CHONs in cloud water.[14–17] However, it is not well understood how the compositions of CHONs are influenced by cloud processes (CPs) due to the complexity of real-world environments. For example, differing reaction mechanisms in cloud water vs. aerosol can lead to differences in CHON compositions between these media.[18] Moreover, cloud cycling between aerosols and cloud droplets induced by water evaporation and condensation, which occur at the minute scale, can lead to the transformation of organic compounds between these two environments.[19] Thus, to

[1]Shanghai Key Laboratory of Atmospheric Particle Pollution and Prevention (LAP[3]), Department of Environmental Science & Engineering, Institute of Atmospheric Sciences, Fudan University, Shanghai 200438, China
[2]State Key Laboratory of Environmental Chemistry and Ecotoxicology, Research Center for Eco-Environmental Sciences, Chinese Academy of Sciences, Beijing 100085, China
[3]Department of Chemistry, College of Natural Sciences, Colorado State University, Fort Collins, CO 80523, USA
[4]University of Lyon, Université Claude Bernard Lyon 1, CNRS, IRCELYO, 69626 Villeurbanne, France
[5]School of Environmental Science and Engineering, Research Institute of Environment, Shandong University, Qingdao 266237, China
[6]Key Laboratory of Environmental Remediation and Ecological Health, Ministry of Education, College of Environmental and Resource Sciences, Zhejiang University, Hangzhou 310058, China
[7]Institut de Combustion, Aérothermique, Réactivité et Environnement, CNRS, 45071 Orléans Cedex 02, France
[8]Institute of Eco-Chongming (IEC), 3663 N. Zhongshan Road, Shanghai 200062, China
[9]These authors contributed equally
[10]Lead contact
*Correspondence: tingruan@rcees.ac.cn (T.R.), jmchen@fudan.edu.cn (J.C.)
https://doi.org/10.1016/j.isci.2023.108317

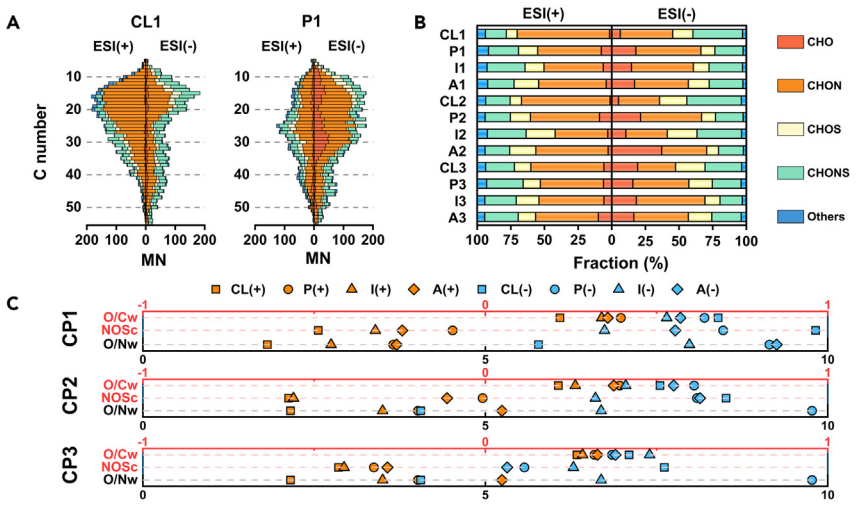

Figure 1. Overview of molecular characteristics of cloud water and aerosols

(A) Molecular number (MN) of every subgroup (CHO, CHON, CHONS, CHOS, and Others) for all of hte samples collected during the three CPs analyzed in ESI (+) and ESI (−).

(B) C number distributions for cloud water (CL1) and aerosol (A1) samples analyzed in ESI (+) and ESI (−).

(C) The nominal oxidation state of the carbon (NOS_C), weighted O/N ratios (O/N_W), and weighted O/C ratios (O/C_W) for all of the samples colelcted during the three CPs and analyzed in ESI (+) and ESI (−).

comprehensively understand how cloud processes influence CHON compositions, more information about CHONs in cloud water, pre-cloud aerosols, interstitial (unscavenged) aerosol, and cloud-processed aerosols, along with their evolution mechanisms is needed.

In this study, we obtained detailed molecular information about CHONs in aerosols and cloud water during CPs (before, during, and after cloud events) using both positive and negative ion modes of a Fourier transform-ion cyclotron resonance mass spectrometry (FT-ICR-MS). We compared the molecular composition of CHONs in aerosols and cloud water and investigated the formation pathways of CHONs in the aqueous phase. Our observations reveal the complexity of CHONs, highlighting distinct molecular characteristics in aerosols vs. cloud water and their chemical transformation. Our findings underscore the importance of aqueous-phase reactions, particularly ammonia–organic reactions during CPs, helping fill a gap in our understanding of the transformation of molecular CHON species between aerosols and clouds.

RESULTS

During the research campaign (on the summit of Mt. Tai, 37°18′ N, 117°13′ E, 1534 m a.s.l.; Figures S1A and S1B) in summers of 2018 and 2021 (Figure S1C), both cloud water and aerosol samples were collected synchronously during CPs. Three cloud water samples and nine aerosol samples were collected during three complete CP events (CP1, CP2, and CP3) (Figure S1C). Nine individual cloud water samples were also collected during nine additional CPs (Table S3). Sample CL1 is the cloud water sample, and samples P1, I1, and A1 are the aerosol samples collected before, during (interstitial), and after event CP1 (Figure S1C), respectively. The details of the sample collection are described in the Methods Section.

All of the samples were analyzed via FT-ICR-MS. The identified molecular formulas were grouped into five subgroups: CHO, CHON, CHOS, CHONS, and others. An average of 3615 and 4478 molecular formulas in the cloud water and 3379 and 4987 in the aerosols were identified in electrospray ionization (ESI) (+) and ESI (−), respectively (Table S3). The C number distributions of CL1 and P1 are shown as examples in Figure 1A to illustrate the difference in the two ion modes, which are centered at 23.6 ± 9.3 and 26.8 ± 12.6 for CL1 and 27.1 ± 10.3 and 27.08 ± 13.6 for P1 in ESI (+) and ESI (−), respectively. $C_{10\text{-}25}$ compounds dominate in CL1, accounting for 62% and 55% of ESI (+) and ESI (−), respectively. High C number compounds account for a larger proportion in P1. Compounds with C numbers greater than 25 account for 53% and 47% of P1 in ESI (+) and ESI (−), respectively, 15% and 2% greater than in CL1. Although numerous previous studies of CHONs have used ESI (−) to study molecular formulas,[20–22] we found that the CHONs in the cloud water in ESI (+) accounted for an average of 63% of all identified formulas 2946 formulas), much more than 1423 (33%) in ESI (−) (Figure 1B). As shown in Figure 1C, in the cloud water and aerosol, the CHONs detected in ESI (+) have lower oxidation states than those detected in ESI (−). The average O/N_w ratios of the CHONs in ESI (+) are 2.3 and 3.8 for the three cloud water samples and nine aerosol samples, respectively, for the CPs, which are lower than those in ESI (−) (4.9 and 8.4) (Table S4). This implies that the CHONs detected in ESI (+) generally have lower oxygen contents.

Variations in molecular features of nitrogenous organics during cloud processes

It is useful to investigate the evolution of CHONs using ESI (+) since it detects more molecular formulas in the cloud water samples than ESI (−). For example, as shown in Figures 1A and S3, the number of CHON molecular formulas in ESI (+) was about twice as large as the number in

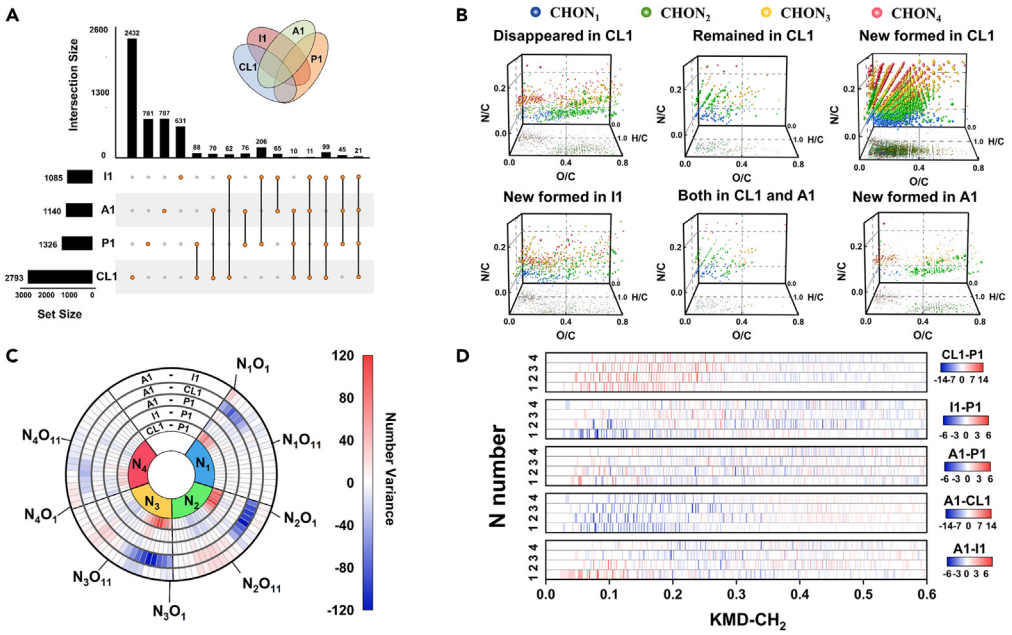

Figure 2. Variations in molecular characteristics of CHONs during CPs

(A) Upset plot of CHONs in the four samples collected during CP11 (P1, CL1, I1, and A1) ans analyzed in ESI (+). The stacked bar plot (top) shows the number of CHONs detected in one or more of these samples. The matrix later in discussion the bar plot indicates which sets of samples are represented by each bar. The bar plots on the left show the total number of CHONs in every sample.

(B) 3-D Van Krevelen (V-K) diagram of CHONs that disappeared in CL1 compared with P1, the CHONs that remained in CL1 campared with P1, the newly formed CHONs in CL1 compared with P1, the newly formed CHONs in I1 compared with P1, the CHONs that remained in A1 after water evaporation, and the newly formed CHONs in A1 compared with CL1 and I1.

(C) The CHONs were grouped into different subgroups according to their N and O numbers, and the figure shows the number variance of the CHON subgroups between the different samples. From the inside to the outside, the five rings denote the number in CL1 minus the number in P1, the number in I1 minus the number in P1, the number in A1 minus the number in P1, the number in A1 minus the number in CL1, and the number in A1 minus the number in I1.

(D) The CHONs were grouped into different subgroups according to the KMD-CH_2 value, and the figure shows the number variance of the CHON subgroups between the different samples. From the top to the bottom, the values are the number in CL1 minus the number in P1, the number in I1 minus the number in P1, the number in A1 minus the number in P1, the number in A1 minus the number in CL1, and the number in A1 minus the number in I1.

ESI (−) for the cloud water samples, accounting for 69%, 66%, and 54% in ESI (+) for CL1, CL2, and CL3, respectively. As shown in Figure 2A, the UpSet plot for CP1 was generated to visualize intersecting formula sets across the four samples. CL1 had the largest number of unique formulas 2432, around three times as large as the three aerosol samples for this event. P1 and A1 had the largest number of common formulas in the pairwise intersection. CL1 and P1 only had 218 formulas in common, indicating the large difference in the chemical compositions of the cloud water and aerosols. Similar results were obtained for the other two CP events, indicating that abundant CHONs formed in the cloud water (Figure S4).

To explain the compositions of the CHONs, the identified CHON formulas were separated into subsets based on the numbers of oxygen and nitrogen atoms in the molecular formulas (CHO_xN_y), where x and y represent the numbers of oxygen and nitrogen atoms, respectively. Figures 2B and 2C, and 2D provide insights into the formation and transformation of CHONs during CP1, representing the changes in CHONs from the pre-cloud samples (P1) to the in-cloud samples (CL1 and I1) and finally to the after-cloud samples (A1). Figure 2B displays the N/C, O/C, and H/C ratios of the CHONs via a 3-D Van Krevelen (VK) diagram, which is size-coded based on the molecular signal intensity. After cloud formation, the parts of the CHONs that are absent from the cloud water exhibited two different features. $CHON_3$ and $CHON_4$ compounds with low oxidation states (O/C < 0.2) and high unsaturation (H/C < 1.5) were detected in P1 but not in CL1. The features of these CHONs were consistent with humic-like substances emitted during biomass burning and coal combustion.[23] The other P1 CHONs absent from CL1 had extremely different features, with significantly higher O/C and H/C ratios (O/C > 0.3; H/C > 1) which is similar with CHONs in ESI (−). A previous study also reported the occurrence of some CHONs with O/N ratios of >3 in both ESI (+) and ESI (−), and these CHONs may contain both oxidized nitrogen and acidic groups.[23] The P1 CHONs that remained in CL1 after cloud formation were mainly $CHON_1$ and $CHON_2$ compounds, and they had similar formula features to CHONs newly formed in the cloud water. These CHONs plot in the 0 < O/C < 0.5, 1 < H/C < 2.2, and 0.1 < N/C < 0.3 region and exhibit radial distributions on the 3-D VK diagram. The number of new CHONs identified in I1 was much less than in the cloud water, consistent with previous findings obtained via aircraft sampling[24] suggesting that the formation of CHONs in cloud water is more important than in aerosols. The newly formed CHONs in I1 plot in a similar region (0 < O/C < 0.5, 1 < H/C < 2.2, and 0.1 < N/C < 0.3) to those in CL1, likely due to partitioning or cycling between the cloud droplets and

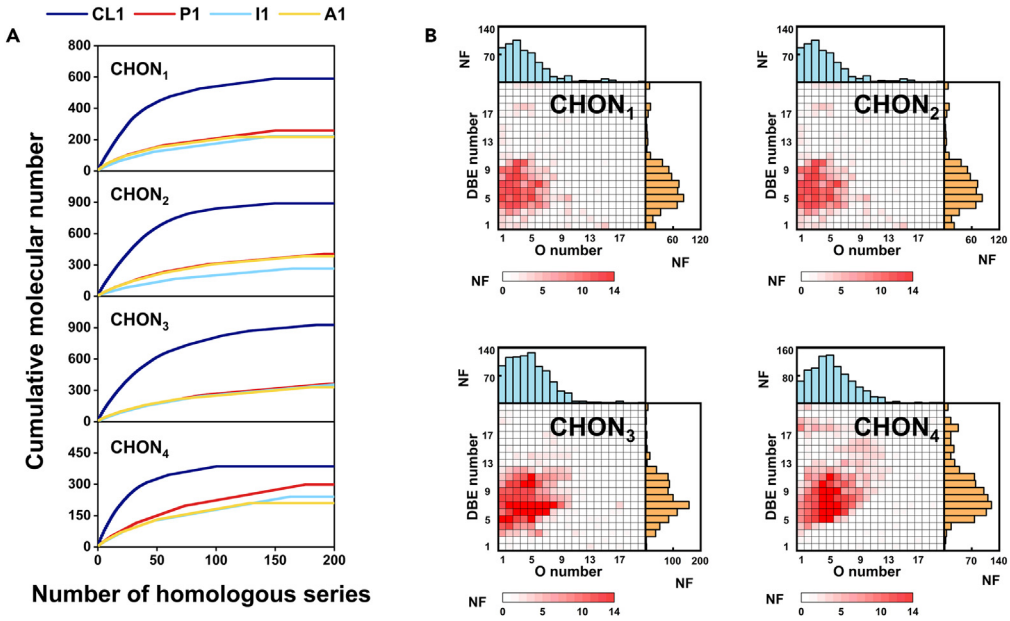

Figure 3. Molecular compositions of CHONs in cloud water

(A) The CHONs were grouped into four subgroups accordance to the N number and were further grouped into different classes accroding to the KMD-CH_2 value (a class of homologous series). The number of CHONs with each added homologous series for every subgroup in CL1, P1, I1, and A1.

(B) Heatmap showing the DBE and O number distributions of the CHONs in CL1. The color scale represents the number of formulas (NF) for each combination of DBE and O number, which corresponds to the number of formulas within a specific Kendrick series based on CH_2.

interstitial aerosols. After cloud evaporation, some of the newly formed compounds in CL1 may have remained in A1. However, some CHONs observed in A1 were very similar to those in P1. These results may be limited by the fixed sampling location and changing atmospheric environment across the cloud event. Further field observations should focus on the influence of CPs on aerosols after cloud events.

Overall, Figure 2 shows that the CHONs containing reduced nitrogen functional groups rather than nitro or nitrooxy groups were one of the main characteristics of the cloud water. Thus, more attention should be paid to investigate the evolution of oxygen distributions in CHONs during CP events. Here, the CHONs were further classified into 80 subgroups (including $N_{1–4}O_{1–20}$; Figure 2C) according to the numbers of nitrogen and oxygen atoms. Figure 2C provides insights into the variations in the molecular numbers for every CHON subgroup among the different samples. Substantial differences in the number of CHONs in every subgroup between CL1 and P1 were observed. Compared with P1, CL1 had a high number of CHONs, and they were mainly distributed in the oxygen number $\leq$10 group, including $N_1O_{1–5}$, $N_2O_{1–7}$, and $N_3O_{1–9}$. The number of CHONs in the oxygen number >10 group were less abundant in CL1. A similar decrease in the higher oxygen number CHONs was also observed in I1, but there was no noticeable increase in the number of CHONs in the lower oxygen subgroups. After cloud water evaporation, the variation patterns from A1 to CL1 and from A1 to I1 were opposite to those from CL1 to P1 and from I1 to P1, which can be seen from the small variance in the number of CHONs in every subgroup between P1 and A1. The Kendrick mass defect (KMD) plots (Figure 2D) provide more molecular information about the different samples and are color-coded by the number difference with the same KMD value. Generally, a series of homologues have the same KMD-CH_2 value. A unit increase in the number of O atoms, number of N atoms, and double bond equivalent (DBE) values will result in increases of 0.023, 0.006, and 0.013 in the KMD-CH_2 value for CHONs. The KMD-CH_2 values of the CHONs that increased in CL1 were less than 0.3 since they had fewer O atoms, while the CHONs that were abundant in P1 and A1 had KMD values of greater than 0.3.

Molecular compositions of nitrogenous organics in cloud water

As was discussed above, many CHONs containing reduced nitrogen functional groups were detected in the cloud water. A series of homologues are more likely to have similar features, and every CHON subgroup ($CHON_1$, $CHON_2$, $CHON_3$, and $CHON_4$) can be classified into ~200 homologue series. To evaluate the distributions of the CHONs in the cloud water and aerosols, we calculated every CHON subgroup's accumulation curve for CL1, P1, I1, and A1 for CP1 (Figure 3A) and for the other two CP events (Figure S8). Despite the diversity of the molecular compositions of the CHONs and the large number of CHONs detected in the cloud water, the molecular accumulation across every subgroup of CHONs in the cloud water exhibited a rapid increase, with top 50 CHON homologous series accounting for 80% of the CHONs. This indicates that a large fraction of the cloud water CHONs had similar characteristics and the CHONs detected in the cloud water can be summarized using specific molecular formulas. Figure 3B shows the DBE and C number distributions for the four CHONs subgroups in CL1. The color represents the number of formulae within the specific homologue series of CHONs. For all of the CHONs in the cloud water (Figures 3B and S8), 72% $\pm$ 11% of the CHONs had O numbers of 1–10 and DBE values of 2–10, which can be described by the formula

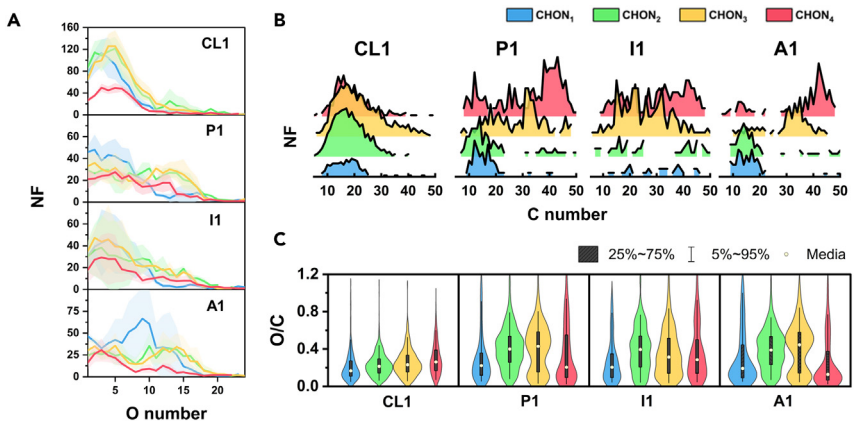

Figure 4. Different CHON formation pathways in cloud water and aerosols

(A) O number distributions for every CHON subgroup for CL1, P1, I1, and A1. The dash line representes average O number and the shaded area represent the standard deviation (B) C number distributions with increasing N number for the CHONs with O/N ratios of less than 3.

(C) O/C ratio distributions of CHONs with increasing N number.

$C_nH_{(2n-16)-(2n)}O_{1-10}N_{1-4}$. We noticed that adding one more nitrogen atom did not influence the DBE value and O number distributions, further supporting the small possibility of the nitro or nitrooxy groups acting as nitrogen atom sources. The CHONs emitted during biomass burning and coal combustion are similar to the molecular characteristics observed in this study [23 25]. For example, most of these CHONs were preferentially detected in ESI (+) and had lower O/N ratios. It was found that the CHONs had higher DBE values as the N number increased, indicating that these CHONs may have consisted of aromatic N-heterocyclic compounds. However, the similar distributions of the DBE values of the different CHON subgroups observed in this study illustrate that there were more likely other nitrogen base functional group containing compounds such as amines rather than aromatic N-heterocyclic compounds.

Different molecular characteristics of nitrogenous organics in cloud water and aerosols

To explore and compare the CHON formation pathways in cloud water and aerosols, we further compared the molecular characteristics of the CHONs with the variation in the N number in the cloud water and aerosols. The O number distribution with the increasing number of nitrogen atoms is shown in Figure 4A, and the weighted O number (O_w) of every CHON subgroup in all of the samples is listed in Table S4. Unlike the similar O number distributions of the different CHON subgroups in the cloud water, the O number distributions in the aerosols exhibited significantly different patterns. The weighted O numbers increased from 5.32, 4.41, and 6.21 in the $CHON_1$ compounds to 9.02, 9.00, and 9.82 in the $CHON_2$ compounds in the P, I, and A samples, respectively (Table S4), suggesting the presence of one more nitrooxy group in the $CHON_2$ compounds. On average, 53% and 73% of the $CHON_3$ compounds in the P and A samples had O numbers greater than nine, which allowed for the existence of up to three nitrooxy groups. The limited O number of the $CHON_4$ compounds in the aerosols suggests that CHONs with more than three nitrooxy groups are difficult to observe in the atmosphere. Similar O_w values were observed in the $CHON_4$ compounds in the cloud water and aerosol samples (4.57, 6.23, 6.17, and 5.99 in CL, P, I, and A samples, respectively) (Table S4). However, it is unlikely that the cloud water and aerosol CHONs shared similar molecular structures and formation pathways given large differences in their DBE values (7.79, 13.77, 12.06, and 14.01 for the CL, P, I, and A samples, respectively) (Table S4).

To explore CHONs more likely to be assigned to amines in the different samples, the CHONs with O/N ratios of less than three were filtered, and their C distributions are shown in Figures 4B and S9. CL1 exhibited a unimodal C number distribution, with C numbers of 10–30. Notably, the lower-C number CHONs were prominent in all of the CHON subgroups in CL1, and the C number did not obviously increase from $CHON_1$ to $CHON_4$, which indicates that these multi-nitrogen organic compounds were not formed through oligomerization. Unlike the cloud water, the CHONs in the aerosols had no noticeable C distribution features, exhibiting a wider distribution. To examine whether the increase in the O number of the multi-nitrogen organic compounds in the aerosols contributed to the increase in the C number and/or the existence of nitrooxy functional groups, the O/C distributions of the $CHON_{1-4}$ compounds in CP1 were plotted in Figure 4C. The O/C_W values of all of the samples are listed in Table S4. It is obvious that half of the $CHON_{2-3}$ compounds had O/C ratios of greater than 0.4, while nearly all of the CHONs in the cloud water had lower O/C ratios, indicating that the aerosol CHONs were more likely to contain nitrooxy functional groups.

DISCUSSION

Reaction between NH_3 and carbonyls as a possible pathway for the formation of numerous nitrogenous organics in cloud water

2575 CHONs with a wide molecular distribution were detected in cloud water but not in the pre-cloud aerosol, suggesting they may have formed through aqueous chemistry. Several mechanisms have been proposed to explain the formation of abundant nitrogenous bases in the atmosphere. Wang et al.[25] explained the formation of CHONs with m/z values of 250–500 detected in ESI (+) through the Mannich

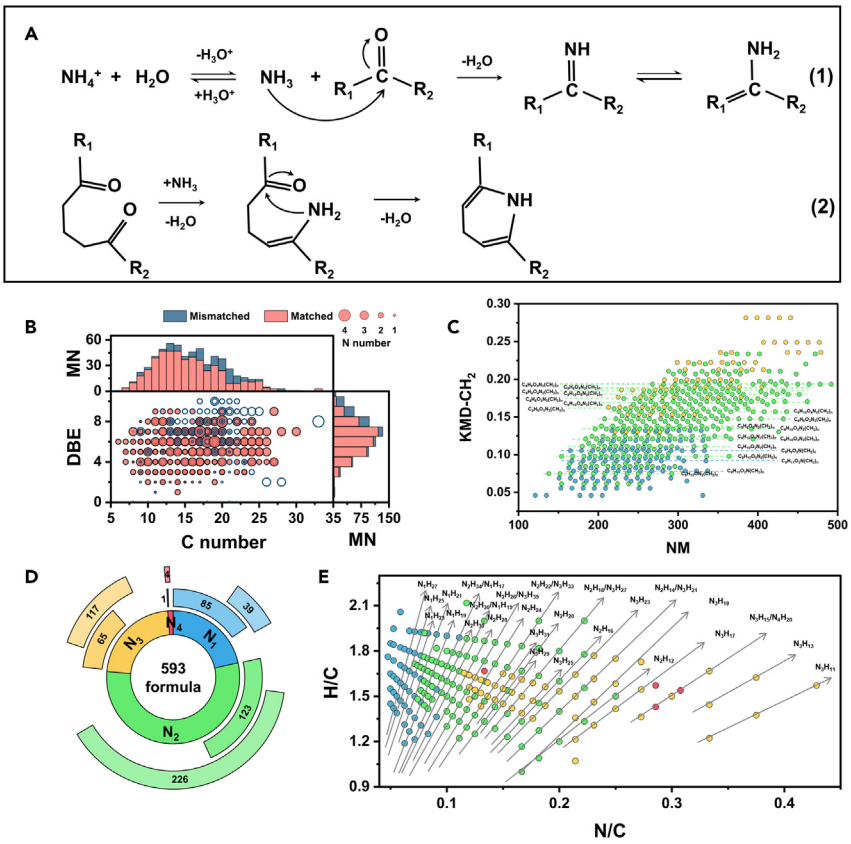

Figure 5. Potential formation scheme of CHONs in cloud water

(A) Schematic diagram of reactions between carbonyl compounds and ammonia that form CHONs. Reaction 1 was assigned to the amine pathway, i.e., the reaction of aldehydes or ketones with ammonia results in the formation of imines. Reaction 2 was assigned to the intramolecular N-heterocycle pathway, i.e., the imine group can undergo reactions with carbonyls present in the skeleton of the same molecule, forming nitrogen-containing heterocyclic compounds.

(B) C number and DBE distributions of the 593 CHONs that were detected in at least half of the cloud water samples. The pink and blue symbols denote the CHONs that can and cannot be explained by scheme A (1).

(C) Kendrick plots of the 593 CHONs based on the CH_2 homologue series. Note that only the Kendrick series with at least five members were plotted.

(D) The number of CHONs and their precursors that can be explained by scheme A (1). The inner ring represents the numbers of the four CHON subgroup of the 593 CHONs. The second ring represents the number of CHO compounds in the samples that act as precursors. The outer ring represents the number of BVOC ozonation products listed as precursors in the literature.

(E) Van Krevelen diagram of H/C vs. N/C for the 459 CHONs that can be explained by scheme A (1).

reaction, i.e., the reaction of NH_3 or amines with aldehydes to form iminium cations and compounds with a carbonyl functional group that can tautomerize to enols (OH–C=C), which will attack the iminium ions to form Mannich bases. However, this mechanism occurs under acidic conditions (pH value of around 2). The acidity of the cloud water on Mt. Tai significantly decreased from a pH of 3.86 during 2007–2008[26] to 5.87 in 2014[27] and ranged from 5.62 to 6.69 during the sampling campaign. Thus, it is unlikely that the Mannich reaction was the major formation pathway of the CHONs in measured Mt. Tai cloud water. Acid–base reactions between NH_3 or amines and carboxylic acids can lead to the formation of CHONs.[28–30] These reaction products should contain two additional O atoms for every additional N atom, with a corresponding increase in the O/C ratio. As was discussed above, the O_w and O/C ratios did not increase sufficiently with the increasing number of N atoms in the CHONs in the cloud water (Figure 4) to support the acid–base reactions as the main CHON formation pathway. A series of recent laboratory simulations have shown that NH_4^+ or amines can react with carbonyls to generate CHONs via nucleophilic attack.[31–37] Thus, we propose that reactions with NH_4^+ and carbonyls are a possible pathway for forming the numerous CHONs in the cloud water. This mechanism is likely to be more consistent with the results of this study and is discussed in detail later in discussion.

A proposed mechanism of carbonyl compounds and ammonia to form CHONs during CPs is showed in Figure 5, aqueous-phase NH_3 is in equilibrium with NH_4^+, and an aldehyde or ketone can undergo nucleophilic attack by NH_3 followed by the loss of water, producing iminium intermediates or converting to enamines (C=C–N).[38] Multi-carbonyl compounds can react with more than one NH_3 to form compounds with multiple amine groups. A carbonyl group could react with NH_3 to form an enamine group and can further react with another carbonyl group in the same molecule, resulting in nitrogen-containing heterocyclic compounds (Figure 5A(2)).[39] This is consistent with the molecular characteristics of the CHONs in the cloud water discussed above, where the C number exhibits a unimodal distribution and the O/C ratios maintain a

similar range with increasing N number. CHONs with high O numbers were observed in the aerosols, exhibiting different molecular features than in the cloud water, indicating that CHONs in the cloud water and aerosols have different characteristics and formation mechanisms. We found that the CHONs in the interstitial aerosol sample (I) had lower O/C_w ratios than those in P and A for all three CP events. This may reflect transformation from cloud water to I through water evaporation.

Low acidic conditions and evaporation could accelerate the formation of nitrogenous organics

Acidity has been proven to significantly affect the formation of nitrogen-containing compounds through the reaction of carbonyls and NH_3. Previous studies have reported that the reaction between carbonyls and NH_4^+ in bulk solutions was inhibited under acidic conditions (pH < 4).[23,24,38] Nguyen et al.[4] found that CHONs were formed at pHs of 4–9 during cloud evaporation, and organosulfates produced by acid-catalyzed aldol condensation were the main products when the pH value was <2. Cloud water has a wide range of pH values[40] and is very sensitive to anthropogenic emissions of sulfur and nitrogen oxides and ambient ammonia. Previous observations on Mt. Tai indicate that the pH of the cloud water decreased from a mean value of 3.86 in 2007 to 6.4 during this study, benefiting from the control of sulfur and nitrogen oxide emissions.[26,27,41] The more neutral pH is advantageous to the reaction between carbonyls and NH_3 and inhibits acid-catalyzed reactions such as aldol condensation,[42–45] hemiacetal and acetal formation,[24,46,47] and esterification of carboxylic acids.[48] Lian et al.[49] provided field evidence of the formation of CHONs through reactions between carbonyls and NH_4^+/amines during a CP event on Mt. Tianjing. They reported that the cloud pH on Mt. Tianjing was 4.13–4.37 [14], considerably lower than that observed here on Mt. Tai. Particle acidities remain relatively constant under lower sulfur and nitrogen oxide concentrations, likely due to the semivolatile nature of small molecular acids and bases and the buffering within particles.[40] Liu et al.[50] reported that the fine particle pH on Mt. Tai was 3.6 $\pm$ 0.7 during the summer of 2018. The difference in the acidity of the aerosols and cloud water may help explain the different molecular characteristics and formation pathways of CHONs.

CHON formation could be accelerated by evaporation, as demonstrated by previous laboratory simulations. Nguyen et al.[4] reported that water evaporation from organic aerosol generated from ozonolysis of *d*-limonene in the presence of $(NH_4)_2SO_4$ could increase the formation rate of CHONs by at least three orders of magnitude compared to that in a bulk aqueous solution. De Haan et al.[51] demonstrated that CHONs could be formed on a timescale of several minutes via reactions between methylglyoxal and amino acids, methylamine, and $(NH_4)_2SO_4$ in simulated evaporating cloud droplets. Lee et al.[5] found that the evaporation of glyoxal-ammonium salt droplets could quickly produce CHONs on a timescale of several seconds, several orders of magnitude faster than observed in bulk solutions. The above results prove that droplet evaporation could accelerate the formation rate of CHONs, likely due to the formation of a highly concentrated solute environment on a relatively short timescale (on the order of seconds), which could explain the formation of numerous CHONs in cloud water. All of the above-described laboratory simulations were performed based on bulk solutions, and further simulations related to the reaction rates in evaporated droplets should be explored. It is also important to keep in mind that the chemical composition and acidity of drops within a given cloud parcel can vary,[52,53] due in part to the nucleation of cloud drops on an externally mixed aerosol population, so that different reaction regimes might exist simultaneously across a population of droplets.

Major newly formed nitrogenous organics in cloud water and their potential precursors

The CHONs widely observed in cloud samples were selected to further examine their potential formation process through reactions between NH_3 and carbonyls. A total of 593 CHONs with O/N ratios of less than 3 and that occurred in at least half of the cloud samples ($\geq$ 6samples) were analyzed (Figures 5B–5E; and Table S5). Most of these CHONs had 8–25 C atoms and DBE values of 3–10. These CHONs were grouped into 103 homologous groups. To more clearly interpret the Kendrick series compositions of the CHONs, at least five consecutive members in every series plotted on the Kendrick plots are shown in Figure 5C. More details about their molecular features are presented in Table S5. These CHON molecules were assumed to be the products of the above formation pathways, which were conversely inferred to obtain the corresponding carbonyl precursors. The ubiquitous existence of alkenes and the high ozone concentration on Mt. Tai enhance the possibility of carbonyl formation and the further generation of CHONs in the cloud water. The gas-phase oxidation of alkenes by ozone has been elucidated in previous studies.[54] In general, the initial step proceeds through the cycloaddition of ozone to the C=C bond, forming an excited primary ozonide. The primary ozonide undergoes unimolecular isomerization to produce Criegee intermediates, which can subsequently yield carbonyls and can transfer to the liquid or particle phase. Alkene ozonolysis also occurs in the liquid phase, which forms an intermediate molozonide in a 1,3-dipolar cycloaddition first and then reverts to its corresponding carbonyl oxide. In particular, cycloolefin such as limonene can be oxidized to yield a chain containing two carbonyls.[55] About 80% of the land on Mt. Tai is covered by vegetation, which releases large amounts of biogenic volatile organic compounds (BVOCs), including isoprene, monoterpenes, and sesquiterpenes.[56,57] In the summer, the average concentrations of isoprene, α-pinene, and β-pinene on Mt. Tai have been measured to be 150, 76, and 18 pptv, respectively.[58] Previous work suggests that OH radicals make a larger contribution to isoprene oxidation in the atmosphere, while the terpenes are mainly oxidized by ozone.[59] Thus, it is reasonable to speculate that terpene ozone oxidation products widely exist on Mt. Tai. Except for the terpene ozone oxidation products, the CHO compounds detected in the cloud water had high DBE values, suggesting the presence of carbonyl groups. We summarized the terpene ozone oxidation products in previous laboratory simulations and the CHO compounds that were detected in at least half of the cloud samples ($\geq$ 6samples) as precursors. To avoid overestimating the contribution of this formation pathway, only a matching algorithm based on the reaction channel in Figure 5A(1) was calculated. As Figure 5D shows, a total of 459 CHONs can be satisfactorily explained by this matching algorithm. The global contribution of BVOCs was estimated to be 66% (n = 393). The most significant contributor from biogenic sources was identified as α-pinene, which contributed 67-72% to the formation of the CHONs. *d*-limonene and

isoprene contributed 6–11% and 5%, respectively. Similarly, atmospheric organic amines such as monomethylamine (MMA) and dimethylamine (DMA) may also have contributed to the formation of the CHONs. Due to the relatively low concentrations of amines in the atmosphere, the contribution of the amines was not taken into further consideration. The Van Krevelen diagram of H/C vs. N/C for all of the matched CHONs is presented in Figure 5E. The majority of these compounds had N/C ratios of 0.05–0.3.

The field observations discussed in this article demonstrate the great differences in the molecular characteristics of CHONs between aerosols and cloud water. We propose that CP events have an important impact on CHON formation mechanisms, highlighting the importance of inorganic–organic interactions in cloud water. Different acidity regimes and microphysical conditions may lead to different dominant chemical processes. Significant decreases in the emission of sulfur and nitrogen oxide acid precursors can decrease the acidity of cloud water, which may increase the importance of ammonia-organic reactions. In addition, the cycling between aerosols and cloud water through condensation and evaporation may also lead to the transfer of compounds between these two regimes.[55] Chemical reactions during CP events can also have an important impact on radiative forcing and climate such as the browning reaction with ammonium salts to form organic carbon with C-N/C=N functionalities capable of absorbing ultraviolet (UV) radiation, a pathway known to be a potential source of brown carbon.[60] In-depth analysis of the chemical reactions during CP events focusing on inorganic–organic reactions and the cycling and transformation of compounds between cloud water and aerosols warrants further research.

Limitations of the study

We note that real atmosphere environment is significant different from simulated experiment. Due to the fluidity of air, the sample was affected by extraneous air, which affects their compounds compositions. Estimating the contribution of cloud process to aerosol composition is challenging. We call for more research into cloud processes in more complicated environmental conditions, such as varying wind velocity, anthropogenic input. In these ways, it would be possible to develop models for predicting the formation of CHON during cloud processes. Moreover, due to the limitation of FT-ICR-MS, this study can only identify the same compound through equally m/z ratio and isomers were not taking into account. Chromatographic separation prior to MS analysis, coupled with simulation studies using model carbonyls, should provide additional mechanistic evidence to our proposed pathways.

STAR★METHODS

Detailed methods are provided in the online version of this paper and include the following:

- KEY RESOURCES TABLE
- RESOURCE AVAILABILITY
  - Lead contact
  - Materials availability
  - Data and code availability
- METHOD DETAILS
  - Sample collection
  - Sample preparation
  - FT-ICR-MS analysis
  - Data processing and formula assignment
- QUANTIFICATION AND STATISTICAL ANALYSIS

SUPPLEMENTAL INFORMATION

Supplemental information can be found online at https://doi.org/10.1016/j.isci.2023.108317.

ACKNOWLEDGMENTS

Ministry of Science and Technology of the People's Republic of China (2022YFC3701101).
National Natural Science Foundation of China (Nos. 22336001, 91843301, 21527814).
Science and Technology Commission of Shanghai Municipality, China (No. 21DZ1202300).
Shanghai International Science and Technology Partnership Project (No. 21230780200).
European Union's Horizon 2020 research and innovation program (MARSU, 690958).

AUTHOR CONTRIBUTIONS

J.C. conceived the idea and study design; Z.L., B.Z., C.Z., and J.L. collected and analyzed data; Z.L., B.Z., and C.Z. wrote the article; J.C., T.R., H.C., and Q.L. supervised the article; and all authors discussed the results and approved the article.

DECLARATION OF INTERESTS

The authors declare that they have no competing interests.

Received: July 18, 2023
Revised: September 4, 2023
Accepted: October 20, 2023
Published: October 24, 2023

REFERENCES

1. Hao, L., Romakkaniemi, S., Kortelainen, A., Jaatinen, A., Portin, H., Miettinen, P., Komppula, M., Leskinen, A., Virtanen, A., Smith, J.N., et al. (2013). Aerosol Chemical Composition in Cloud Events by High Resolution Time-of-Flight Aerosol Mass Spectrometry. Environ. Sci. Technol. *47*, 2645–2653. https://doi.org/10.1021/es302889w.
2. McNeill, V.F. (2015). Aqueous Organic Chemistry in the Atmosphere: Sources and Chemical Processing of Organic Aerosols. Environ. Sci. Technol. *49*, 1237–1244. https://doi.org/10.1021/es5043707.
3. Ervens, B., Turpin, B.J., and Weber, R.J. (2011). Secondary organic aerosol formation in cloud droplets and aqueous particles (aqSOA): a review of laboratory, field and model studies. Atmos. Chem. Phys. *11*, 11069–11102. https://doi.org/10.5194/acp-11-11069-2011.
4. Nguyen, T.B., Lee, P.B., Updyke, K.M., Bones, D.L., Laskin, J., Laskin, A., and Nizkorodov, S.A. (2012). Formation of nitrogen- and sulfur-containing light-absorbing compounds accelerated by evaporation of water from secondary organic aerosols. J. Geophys. Res. *117*. https://doi.org/10.1029/2011JD016944.
5. Lee, A.K.Y., Zhao, R., Li, R., Liggio, J., Li, S.-M., and Abbatt, J.P.D. (2013). Formation of Light Absorbing Organo-Nitrogen Species from Evaporation of Droplets Containing Glyoxal and Ammonium Sulfate. Environ. Sci. Technol. *47*, 12819–12826. https://doi.org/10.1021/es402687w.
6. Wang, X., Hayeck, N., Brüggemann, M., Yao, L., Chen, H., Zhang, C., Emmelin, C., Chen, J., George, C., and Wang, L. (2017). Chemical Characteristics of Organic Aerosols in Shanghai: A Study by Ultrahigh-Performance Liquid Chromatography Coupled With Orbitrap Mass Spectrometry. JGR. Atmospheres *122*, 703–711. 722. https://doi.org/10.1002/2017JD026930.
7. Seinfeld, J.H., Bretherton, C., Carslaw, K.S., Coe, H., DeMott, P.J., Dunlea, E.J., Feingold, G., Ghan, S., Guenther, A.B., Kahn, R., et al. (2016). Improving our fundamental understanding of the role of aerosol−cloud interactions in the climate system. Proc. Natl. Acad. Sci. USA *113*, 5781–5790. https://doi.org/10.1073/pnas.1514043113.
8. Mohr, C., Thornton, J.A., Heitto, A., Lopez-Hilfiker, F.D., Lutz, A., Riipinen, I., Hong, J., Donahue, N.M., Hallquist, M., Petäjä, T., et al. (2019). Molecular identification of organic vapors driving atmospheric nanoparticle growth. Nat. Commun. *10*, 4442. https://doi.org/10.1038/s41467-019-12473-2.
9. An, Z., Huang, R.-J., Zhang, R., Tie, X., Li, G., Cao, J., Zhou, W., Shi, Z., Han, Y., Gu, Z., and Ji, Y. (2019). Severe haze in northern China: A synergy of anthropogenic emissions and atmospheric processes. Proc. Natl. Acad. Sci. USA *116*, 8657–8666. https://doi.org/10.1073/pnas.1900125116.
10. Ravishankara, A.R. (1997). Heterogeneous and Multiphase Chemistry in the Troposphere. Science *276*, 1058–1065. https://doi.org/10.1126/science.276.5315.1058.
11. Lin, P., Laskin, J., Nizkorodov, S.A., and Laskin, A. (2015). Revealing Brown Carbon Chromophores Produced in Reactions of Methylglyoxal with Ammonium Sulfate. Environ. Sci. Technol. *49*, 14257–14266. https://doi.org/10.1021/acs.est.5b03608.
12. Nizkorodov, S.A., Laskin, J., and Laskin, A. (2011). Molecular chemistry of organic aerosols through the application of high resolution mass spectrometry. Phys. Chem. Chem. Phys. *13*, 3612–3629. https://doi.org/10.1039/C0CP02032J.
13. Herckes, P., Valsaraj, K.T., and Collett, J.L. (2013). A review of observations of organic matter in fogs and clouds: Origin, processing and fate. Atmos. Res. *132–133*, 434–449. https://doi.org/10.1016/j.atmosres.2013.06.005.
14. Sun, W., Fu, Y., Zhang, G., Yang, Y., Jiang, F., Lian, X., Jiang, B., Liao, Y., Bi, X., Chen, D., et al. (2021). Measurement report: Molecular characteristics of cloud water in southern China and insights into aqueous-phase processes from Fourier transform ion cyclotron resonance mass spectrometry. Atmos. Chem. Phys. *21*, 16631–16644. https://doi.org/10.5194/acp-21-16631-2021.
15. Zhao, Y., Hallar, A.G., and Mazzoleni, L.R. (2013). Atmospheric organic matter in clouds: exact masses and molecular formula identification using ultrahigh-resolution FT-ICR mass spectrometry. Atmos. Chem. Phys. *13*, 12343–12362. https://doi.org/10.5194/acp-13-12343-2013.
16. Bianco, A., Riva, M., Baray, J.-L., Ribeiro, M., Chaumerliac, N., George, C., Bridoux, M., and Deguillaume, L. (2019). Chemical Characterization of Cloudwater Collected at Puy de Dôme by FT-ICR MS Reveals the Presence of SOA Components. ACS Earth Space Chem. *3*, 2076–2087. https://doi.org/10.1021/acsearthspacechem.9b00153.
17. Mazzoleni, L.R., Ehrmann, B.M., Shen, X., Marshall, A.G., and Collett, J.L., Jr. (2010). Water-Soluble Atmospheric Organic Matter in Fog: Exact Masses and Chemical Formula Identification by Ultrahigh-Resolution Fourier Transform Ion Cyclotron Resonance Mass Spectrometry. Environ. Sci. Technol. *44*, 3690–3697. https://doi.org/10.1021/es903409k.
18. Boone, E.J., Laskin, A., Laskin, J., Wirth, C., Shepson, P.B., Stirm, B.H., and Pratt, K.A. (2015). Aqueous Processing of Atmospheric Organic Particles in Cloud Water Collected via Aircraft Sampling. Environ. Sci. Technol. *49*, 8523–8530. https://doi.org/10.1021/acs.est.5b01639.
19. Tsui, W.G., Woo, J.L., and McNeill, V.F. (2019). Impact of Aerosol-Cloud Cycling on Aqueous Secondary Organic Aerosol Formation. Atmosphere *10*, 666.
20. Lin, P., Rincon, A.G., Kalberer, M., and Yu, J.Z. (2012). Elemental Composition of HULIS in the Pearl River Delta Region, China: Results Inferred from Positive and Negative Electrospray High Resolution Mass Spectrometric Data. Environ. Sci. Technol. *46*, 7454–7462. https://doi.org/10.1021/es300285d.
21. Wang, K., Huang, R.J., Brüggemann, M., Zhang, Y., Yang, L., Ni, H., Guo, J., Wang, M., Han, J., Bilde, M., et al. (2021). Urban organic aerosol composition in eastern China differs from north to south: molecular insight from a liquid chromatography–mass spectrometry (Orbitrap) study. Atmos. Chem. Phys. *21*, 9089–9104. https://doi.org/10.5194/acp-21-9089-2021.
22. Daellenbach, K.R., Kourtchev, I., Vogel, A.L., Bruns, E.A., Jiang, J., Petäjä, T., Jaffrezo, J.L., Aksoyoglu, S., Kalberer, M., Baltensperger, U., et al. (2019). Impact of anthropogenic and biogenic sources on the seasonal variation in the molecular composition of urban organic aerosols: a field and laboratory study using ultra-high-resolution mass spectrometry. Atmos. Chem. Phys. *19*, 5973–5991. https://doi.org/10.5194/acp-19-5973-2019.
23. Nozière, B., Dziedzic, P., and Córdova, A. (2009). Products and Kinetics of the Liquid-Phase Reaction of Glyoxal Catalyzed by Ammonium Ions (NH4+). J. Phys. Chem. A *113*, 231–237. https://doi.org/10.1021/jp8078293.
24. Shapiro, E.L., Szprengiel, J., Sareen, N., Jen, C.N., Giordano, M.R., and McNeill, V.F. (2009). Light-absorbing secondary organic material formed by glyoxal in aqueous aerosol mimics. Atmos. Chem. Phys. *9*, 2289–2300. https://doi.org/10.5194/acp-9-2289-2009.
25. Wang, X., Gao, S., Yang, X., Chen, H., Chen, J., Zhuang, G., Surratt, J.D., Chan, M.N., and Seinfeld, J.H. (2010). Evidence for High Molecular Weight Nitrogen-Containing Organic Salts in Urban Aerosols. Environ. Sci. Technol. *44*, 4441–4446. https://doi.org/10.1021/es1001117.
26. Guo, J., Wang, Y., Shen, X., Wang, Z., Lee, T., Wang, X., Li, P., Sun, M., Collett, J.L., Wang, W., and Wang, T. (2012). Characterization of cloud water chemistry at Mount Tai, China: Seasonal variation, anthropogenic impact, and cloud processing. Atmos. Environ. *60*, 467–476. https://doi.org/10.1016/j.atmosenv.2012.07.016.
27. Li, J., Wang, X., Chen, J., Zhu, C., Li, W., Li, C., Liu, L., Xu, C., Wen, L., Xue, L., et al. (2017). Chemical composition and droplet size distribution of cloud at the summit of Mount Tai, China. Atmos. Chem. Phys. *17*, 9885–9896. https://doi.org/10.5194/acp-17-9885-2017.
28. Liu, Y., Ma, Q., and He, H. (2012). Heterogeneous Uptake of Amines by Citric Acid and Humic Acid. Environ. Sci. Technol. *46*, 11112–11118. https://doi.org/10.1021/es302414v.
29. Kuwata, M., and Martin, S.T. (2012). Phase of atmospheric secondary organic material affects its reactivity. Proc. Natl. Acad. Sci. USA *109*, 17354–17359. https://doi.org/10.1073/pnas.1209071109.
30. Zhang, R., Wang, G., Guo, S., Zamora, M.L., Ying, Q., Lin, Y., Wang, W., Hu, M., and Wang, Y. (2015). Formation of Urban Fine Particulate Matter. Chem. Rev. *115*, 3803–3855. https://doi.org/10.1021/acs.chemrev.5b00067.
31. Marrero-Ortiz, W., Hu, M., Du, Z., Ji, Y., Wang, Y., Guo, S., Lin, Y., Gomez-Hermandez, M., Peng, J., Li, Y., et al. (2019). Formation and Optical Properties of Brown Carbon from Small α-Dicarbonyls and Amines. Environ. Sci. Technol. *53*, 117–126. https://doi.org/10.1021/acs.est.8b03995.

32. Galloway, M.M., Chhabra, P.S., Chan, A.W.H., Surratt, J.D., Flagan, R.C., Seinfeld, J.H., and Keutsch, F.N. (2009). Glyoxal uptake on ammonium sulphate seed aerosol: reaction products and reversibility of uptake under dark and irradiated conditions. Atmos. Chem. Phys. *9*, 3331–3345. https://doi.org/10.5194/acp-9-3331-2009.
33. De Haan, D.O., Corrigan, A.L., Smith, K.W., Stroik, D.R., Turley, J.J., Lee, F.E., Tolbert, M.A., Jimenez, J.L., Cordova, K.E., and Ferrell, G.R. (2009). Secondary Organic Aerosol-Forming Reactions of Glyoxal with Amino Acids. Environ. Sci. Technol. *43*, 2818–2824. https://doi.org/10.1021/es803534f.
34. De Haan, D.O., Tolbert, M.A., and Jimenez, J.L. (2009). Atmospheric condensed-phase reactions of glyoxal with methylamine. Geophys. Res. Lett. *36*, L11819. https://doi.org/10.1029/2009GL037441.
35. Liu, Y., Liggio, J., Staebler, R., and Li, S.M. (2015). Reactive uptake of ammonia to secondary organic aerosols: kinetics of organonitrogen formation. Atmos. Chem. Phys. *15*, 13569–13584. https://doi.org/10.5194/acp-15-13569-2015.
36. Yu, G., Bayer, A.R., Galloway, M.M., Korshavn, K.J., Fry, C.G., and Keutsch, F.N. (2011). Glyoxal in Aqueous Ammonium Sulfate Solutions: Products, Kinetics and Hydration Effects. Environ. Sci. Technol. *45*, 6336–6342. https://doi.org/10.1021/es200989n.
37. Grace, D.N., Sharp, J.R., Holappa, R.E., Lugos, E.N., Sebold, M.B., Griffith, D.R., Hendrickson, H.P., and Galloway, M.M. (2019). Heterocyclic Product Formation in Aqueous Brown Carbon Systems. ACS Earth Space Chem. *3*, 2472–2481. https://doi.org/10.1021/acsearthspacechem.9b00235.
38. Bones, D.L., Henricksen, D.K., Mang, S.A., Gonsior, M., Bateman, A.P., Nguyen, T.B., Cooper, W.J., and Nizkorodov, S.A. (2010). Appearance of strong absorbers and fluorophores in limonene-O3 secondary organic aerosol due to NH4+-mediated chemical aging over long time scales. J. Geophys. Res. *115*, D05203. https://doi.org/10.1029/2009JD012864.
39. Laskin, J., Laskin, A., Roach, P.J., Slysz, G.W., Anderson, G.A., Nizkorodov, S.A., Bones, D.L., and Nguyen, L.Q. (2010). High-Resolution Desorption Electrospray Ionization Mass Spectrometry for Chemical Characterization of Organic Aerosols. Anal. Chem. *82*, 2048–2058. https://doi.org/10.1021/ac902801f.
40. Pye, H.O.T., Nenes, A., Alexander, B., Ault, A.P., Barth, M.C., Clegg, S.L., Collett, J.L., Jr., Fahey, K.M., Hennigan, C.J., Herrmann, H., et al. (2020). The acidity of atmospheric particles and clouds. Atmos. Chem. Phys. *20*, 4809–4888. https://doi.org/10.5194/acp-20-4809-2020.
41. Li, J., Zhu, C., Chen, H., Fu, H., Xiao, H., Wang, X., Herrmann, H., and Chen, J. (2020). A More Important Role for the Ozone-S(IV) Oxidation Pathway Due to Decreasing Acidity in Clouds. JGR. Atmospheres *125*, e2020JD033220. https://doi.org/10.1029/2020JD033220.
42. Nozière, B., and Esteve, W. (2007). Light-absorbing aldol condensation products in acidic aerosols: Spectra, kinetics, and contribution to the absorption index. Atmos. Environ. *41*, 1150–1163. https://doi.org/10.1016/j.atmosenv.2006.10.001.
43. Nozière, B., Dziedzic, P., and Córdova, A. (2010). Inorganic ammonium salts and carbonate salts are efficient catalysts for aldol condensation in atmospheric aerosols. Phys. Chem. Chem. Phys. *12*, 3864–3872. https://doi.org/10.1039/B924443C.
44. Sareen, N., Schwier, A.N., Shapiro, E.L., Mitroo, D., and McNeill, V.F. (2010). Secondary organic material formed by methylglyoxal in aqueous aerosol mimics. Atmos. Chem. Phys. *10*, 997–1016. https://doi.org/10.5194/acp-10-997-2010.
45. Li, Z., Schwier, A.N., Sareen, N., and McNeill, V.F. (2011). Reactive processing of formaldehyde and acetaldehyde in aqueous aerosol mimics: surface tension depression and secondary organic products. Atmos. Chem. Phys. *11*, 11617–11629. https://doi.org/10.5194/acp-11-11617-2011.
46. Jang, M., Czoschke, N.M., Lee, S., and Kamens, R.M. (2002). Heterogeneous Atmospheric Aerosol Production by Acid-Catalyzed Particle-Phase Reactions. Science *298*, 814–817. https://doi.org/10.1126/science.1075798.
47. Loeffler, K.W., Koehler, C.A., Paul, N.M., and De Haan, D.O. (2006). Oligomer Formation in Evaporating Aqueous Glyoxal and Methyl Glyoxal Solutions. Environ. Sci. Technol. *40*, 6318–6323. https://doi.org/10.1021/es060810w.
48. Barsanti, K.C., and Pankow, J.F. (2006). Thermodynamics of the formation of atmospheric organic particulate matter by accretion reactions—Part 3: Carboxylic and dicarboxylic acids. Atmos. Environ. *40*, 6676–6686. https://doi.org/10.1016/j.atmosenv.2006.03.013.
49. Lian, X., Zhang, G., Yang, Y., Lin, Q., Fu, Y., Jiang, F., Peng, L., Hu, X., Chen, D., Wang, X., et al. (2021). Evidence for the Formation of Imidazole from Carbonyls and Reduced Nitrogen Species at the Individual Particle Level in the Ambient Atmosphere. Environ. Sci. Technol. Lett. *8*, 9–15. https://doi.org/10.1021/acs.estlett.0c00722.
50. Liu, P., Zhao, X., Zhang, C., Chen, H., Wang, J., Xue, L., Chen, J., and Mu, Y. (2021). Fine particle pH and its influencing factors during summer at Mt. Tai: Comparison between mountain and urban sites. Atmos. Environ. *261*, 118607. https://doi.org/10.1016/j.atmosenv.2021.118607.
51. De Haan, D.O., Hawkins, L.N., Kononenko, J.A., Turley, J.J., Corrigan, A.L., Tolbert, M.A., and Jimenez, J.L. (2011). Formation of Nitrogen-Containing Oligomers by Methylglyoxal and Amines in Simulated Evaporating Cloud Droplets. Environ. Sci. Technol. *45*, 984–991. https://doi.org/10.1021/es102933x.
52. Bator, A., and Collett, J.L., Jr. (1997). Cloud chemistry varies with drop size. J. Geophys. Res. *102*, 28071–28078. https://doi.org/10.1029/97JD02306.
53. Collett, J.L., Jr., Bator, A., Rao, X., and Demoz, B.B. (1994). Acidity variations across the cloud drop size spectrum and their influence on rates of atmospheric sulfate production. Geophys. Res. Lett. *21*, 2393–2396. https://doi.org/10.1029/94GL02480.
54. Zhang, D., and Zhang, R. (2005). Ozonolysis of α-pinene and β-pinene: Kinetics and mechanism. J. Chem. Phys. *122*, 114308. https://doi.org/10.1063/1.1862616.
55. Nguyen, T.K.V., Zhang, Q., Jimenez, J.L., Pike, M., and Carlton, A.G. (2016). Liquid Water: Ubiquitous Contributor to Aerosol Mass. Environ. Sci. Technol. Lett. *3*, 257–263. https://doi.org/10.1021/acs.estlett.6b00167.
56. Guenther, A., Hewitt, C.N., Erickson, D., Fall, R., Geron, C., Graedel, T., Harley, P., Klinger, L., Lerdau, M., Mckay, W.A., et al. (1995). A global model of natural volatile organic compound emissions. J. Geophys. Res. *100*, 8873–8892. https://doi.org/10.1029/94JD02950.
57. Fu, P., Kawamura, K., Kanaya, Y., and Wang, Z. (2010). Contributions of biogenic volatile organic compounds to the formation of secondary organic aerosols over Mt. Tai, Central East China. Atmos. Environ. *44*, 4817–4826. https://doi.org/10.1016/j.atmosenv.2010.08.040.
58. Zhu, Y., Yang, L., Kawamura, K., Chen, J., Ono, K., Wang, X., Xue, L., and Wang, W. (2017). Contributions and source identification of biogenic and anthropogenic hydrocarbons to secondary organic aerosols at Mt. Tai in 2014. Environ. Pollut. *220*, 863–872. https://doi.org/10.1016/j.envpol.2016.10.070.
59. Calogirou, A., Larsen, B.R., and Kotzias, D. (1999). Gas-phase terpene oxidation products: a review. Atmos. Environ. *33*, 1423–1439. https://doi.org/10.1016/S1352-2310(98)00277-5.
60. Woo, J.L., Kim, D.D., Schwier, A.N., Li, R., and McNeill, V.F. (2013). Aqueous aerosol SOA formation: impact on aerosol physical properties. Faraday Discuss *165*, 357–367. https://doi.org/10.1039/C3FD00032J.
61. Demoz, B.B., Collett, J.L., and Daube, B.C. (1996). On the Caltech Active Strand Cloudwater Collectors. Atmos. Res. *41*, 47–62. https://doi.org/10.1016/0169-8095(95)00044-5.
62. Bianco, A., Deguillaume, L., Vaïtilingom, M., Nicol, E., Baray, J.-L., Chaumerliac, N., and Bridoux, M. (2018). Molecular Characterization of Cloud Water Samples Collected at the Puy de Dôme (France) by Fourier Transform Ion Cyclotron Resonance Mass Spectrometry. Environ. Sci. Technol. *52*, 10275–10285. https://doi.org/10.1021/acs.est.8b01964.
63. Koch, B.P., and Dittmar, T. (2006). From mass to structure: an aromaticity index for high-resolution mass data of natural organic matter. Rapid Commun. Mass Spectrom. *20*, 926–932. https://doi.org/10.1002/rcm.2386.
64. Kendrick, E. (1963). A Mass Scale Based on CH2 = 14.0000 for High Resolution Mass Spectrometry of Organic Compounds. Anal. Chem. *35*, 2146–2154. https://doi.org/10.1021/ac60206a048.
65. Kroll, J.H., Donahue, N.M., Jimenez, J.L., Kessler, S.H., Canagaratna, M.R., Wilson, K.R., Altieri, K.E., Mazzoleni, L.R., Wozniak, A.S., Bluhm, H., et al. (2011). Carbon oxidation state as a metric for describing the chemistry of atmospheric organic aerosol. Nat. Chem. *3*, 133–139. https://doi.org/10.1038/nchem.948.
66. LaRowe, D.E., and Van Cappellen, P. (2011). Degradation of natural organic matter: A thermodynamic analysis. Geochem. Cosmochim. Acta *75*, 2030–2042. https://doi.org/10.1016/j.gca.2011.01.020.

STAR★METHODS

KEY RESOURCES TABLE

REAGENT or RESOURCE	SOURCE	IDENTIFIER
Other		
Reversed-phase Oasis HLB cartridge	Waters	N/A

RESOURCE AVAILABILITY

Lead contact

Further information and requests for resources and reagents should be directed to and will be fulfilled by the lead contact, Jianmin Chen (jmchen@fudan.edu.cn).

Materials availability

This study did not generate new materials.

Data and code availability

- All data reported in this paper will be shared by the lead contact upon request.
- This paper does not report the original code.
- Any additional information required to reanalyze the data reported in this paper is available from the lead contact upon request.

METHOD DETAILS

Sample collection

From July 5 to 20, 2018, and July 18 to August 10, 2021, a total of 21 samples including 12 cloud water samples and nine aerosol samples with aerodynamic diameters $\leq$2.5 μm ($PM_{2.5}$) were collected on the summit of Mt. Tai (37°18′ N, 117°13′ E, 1534 m a.s.l.), the highest point on the North China Plain. The high frequency of cloud events, especially in summer, makes Mt. Tai an ideal site for collecting cloud samples and for studying complete CP events. The cloud water samples were collected using a single-stage Caltech active strand cloud-water collector Version 2 (CASCC2) with a 50% cutoff diameter of 3.5 μm.[61] For aerosol samples, a high-volume air sampler used for $PM_{2.5}$ sampling (HIVOL-CVALD, Thermal Fisher Scientific, USA) was operated at a flow rate of 1.13 m^3/min with quartz fiber filters (Whatman, 20 cm × 25 cm). The quartz fiber filters were pre-baked at 650°C for 4 h to remove any adsorbed impurities. After the sampling, the filters were wrapped in aluminum foil, and the cloud water samples collected in polyethylene bottles were stored at −20°C until further treatment. The filters were weighed using a gravimetric balance method at a constant temperature (25°C) and relative humidity (RH, 50%). During the sampling period, the ozone concentration was measured using a 49i O_3 analyzer (Thermo Scientific, USA). The ammonia concentration was measured using active differential optical absorption spectroscopy (DOAS). The light path between the transmitter and the receiver was 40 m. A beta attenuation and optical analyzer monitor (model 5030 SHARP monitor, Thermo Scientific, USA) were used to monitor the $PM_{2.5}$ levels. An optical fog monitor (model FM1-20, Droplet Measurement Technologies Inc., USA) was used to measure the cloud droplet size distribution. The parameters measured using the above instruments are presented in Figure S2 and the entire work flow are presented in Figure S11.

Sample preparation

The cloud water and aerosol samples for FT-ICR-MS (Research Center for Eco-Environmental Sciences) analysis were prepared via solid-phase extraction (SPE). The details of the methodology have been described in previous studies.[15,62] Approximately 55 mL of cloud water sample was filtered through a 0.22-μm membrane (Pall Corporation, USA, polyethersulfone) and was loaded onto a reversed-phase Oasis HLB cartridge (6 cc, Waters, Milford, MA). The HLB cartridges were pre-activated using consecutive reagents, including 1 mL of isopropyl alcohol, 2 mL of acetonitrile, 2 mL of acidified methanol containing 0.1% formic acid, and 2 mL of aqueous 0.1% formic acid. After the sample was loaded, the cartridge was rinsed with 1.0 mL of ultrapure water to remove any inorganic salts and was dried under vacuum. The sample was eventually eluted using 1.5 mL of acetonitrile and was subsequently concentrated to 500 μL under a gentle nitrogen stream. For the aerosol samples, the filters were cut into small pieces (~0.5 × 0.5 cm) and submerged in 10 mL of ultrapure water for ultrasonic extraction for 10 min. The extraction was repeated three times. After centrifugation, the supernatants were combined and treated using the same SPE procedure as described above. It was expected that the compounds with higher polarity and those with molecular weights of less than 100 Da would be lost during the rinsing process due to insufficient retention on the SPE adsorbent.[62] Both the field blanks and laboratory blanks were prepared using the same procedure. All of the sample extracts were stored at −20°C and were re-filtered prior to instrumental analysis.

FT-ICR-MS analysis

The analysis of the sample extracts was performed using a SolariX Fourier transform ion cyclotron resonance mass spectrometer (Bruker Daltonics, GmbH, Bremen, Germany) equipped with a 15.0-T superconducting magnet and an electrospray ionization (ESI, Bruker) source. All of the samples were analyzed in both ESI (+) and ESI (−) mode. The instrument was externally calibrated using 10-mM sodium formate in 50% isopropyl alcohol solution. The sample extracts were directly injected using a syringe pump with an infusion flow rate of 2 μL/min. The broadband scan mode was selected to achieve an ultrahigh mass resolution power (540,000 full width at half maximum (FWHM) at m/z = 400), and the mass detection range of the full scan was 100–1000 Da. The capillary entrance voltage was set to −4.0 kV and +4.0 kV in ESI (+) and ESI (−), respectively. The endplate electrode voltage was −500 V, and the corona needle current was 3000 nA. The time-of-flight and ion accumulation time were optimized at 0.6 ms and 0.2 s, respectively, to transfer the target ions into the mass analyzer and to minimize the space-charged effects of gathering fewer ions in the ICR cell simultaneously. The mass spectra were recorded based on the accumulation of 200 acquisitions of 4-M data size points.

Data processing and formula assignment

The FT-ICR-MS data were processed using the Bruker Data Analysis software (version 4.0). In order to improve the formula assignment accuracy, internal recalibration was further performed using naturally occurring carboxylic acids of O_4 and O_8 homologous compounds for the mass spectra obtained in the ESI (−). We used our own reference masses of common $CHON_1$ compounds for the internal recalibration of the mass spectra obtained in the ESI (+). After the internal calibration, a mass accuracy of less than 0.4 ppm was acquired. The mass spectra peaks with a signal/noise ratio of greater than 3 and an absolute signal response of greater than 10^6 were applied as the filtering thresholds. The search criterion used in the composition assignment was $C_{0\text{-}70}H_{0\text{-}100}O_{0\text{-}25}N_{0\text{-}4}S_{0\text{-}1}$. The maximum acceptable mass error was set as < 1 ppm. The criteria applied to exclude formulas were as follows: the double bond equivalent (DBE) must be an integer value, DBE/C $\leq$ 1, H/C $\leq$ 2.5, and O/C $\leq$ 1.2. The molecular matching scores and isotope information were taken into consideration if there were multiple candidates. The molecular formulas were assigned to the field and laboratory blanks using the same criteria. All of the molecular formulas assigned in the blank samples with intensities of greater than 10% of the sample intensities were excluded in the following analysis. For a molecular formula of $C_cH_hO_oN_nS_s$, the DBE was calculated using Equation 1.[63]

$$DBE = c - \frac{h}{2} + \frac{n}{2} + 1. \quad \text{(Equation 1)}$$

The Kendrick mass (KM) and Kendrick mass defect (KMD) for CH_2, which were applied to research the homologous series, were calculated using Equations 2 and 3.[64]

$$\text{Kendrick mass}(CH_2) = \text{Observed mass} \times \frac{\text{Nominal mass of } CH_2}{\text{Exact mass of } CH_2}. \quad \text{(Equation 2)}$$

$$\text{Kendrick mass defect}(CH_2) = |\text{Nominal mass-Kendrick mass}(CH_2)|. \quad \text{(Equation 3)}$$

The average carbon oxidation state (OS_c) was calculated using Equation 4.[65]

$$OS_C = 2 \times \frac{o}{c} - \frac{h}{c}. \quad \text{(Equation 4)}$$

The average nominal carbon oxidation state (NOSc) was calculated using Equation 5.[66]

$$NOS_C = \frac{4\text{-}(4 \times c + h\text{-}3 \times n\text{-}2 \times o\text{-}2 \times s)}{c} \quad \text{(Equation 5)}$$

QUANTIFICATION AND STATISTICAL ANALYSIS

The relative intensity (RI) weighted O (O_w), O/C (O/C_w), H/C (H/C_w), DBE (DBE_w), DBE/C (DBE/C_w), and O/N (O/N_w) were calculated using Equation 6.

$$X_w = \sum \quad \text{(Equation 6)}$$

where X_i is the above three parameters, and w_i is the RI of the ith molecular formula.